J. Iron Steel Res. Int. (2019) 26:219–229
https://doi.org/10.1007/s42243-018-0162-8

ORIGINAL ARTICLE

Numerical simulation of flow and solidification in continuous casting process with mold electromagnetic stirring

Bin Yang[1,2] · An-yuan Deng[1,2] · Yang Li[1,2] · Xiu-jie Xu[1,2] · En-gang Wang[1,2]

Received: 18 January 2018 / Revised: 25 September 2018 / Accepted: 27 September 2018 / Published online: 25 October 2018

Abstract
The magnetic, heat transfer and flow phenomenon occurring in the continuous casting process under the mold electromagnetic stirring was further analyzed by solving the 3-D electromagnetic field mathematical model and flow solidification model with finite element method and finite volume method, respectively. The results indicate that the solidified shell thickness located in the effective stirring region fluctuates because of the unsteady scouring under the mold electromagnetic stirring. The maximum rotational velocity is a key parameter to the solidification of the billet when controlling the stirring intensity. When the rotational velocity reaches 0.32 m/s, the mush zone enlarges significantly and the solidification rate is further accelerated. The number of vortexes in the lower recirculation zone is not only two and depends on the stirring parameters. Besides, the secondary flow is closely associated with the solidification. Compared with the results of the model ignoring the influence of solidification on the flow of molten steel, the flow pattern within the lower recirculation region changes dramatically, and thus a coupling analysis of the flow, heat transfer, and solidification is essential when simulating the electromagnetic continuous casting process.

Keywords Continuous casting · Electromagnetic stirring · Solidification · Numerical simulation · Flow

1 Introduction

The mold electromagnetic stirring (M-EMS) has been widely used in the continuous casting process to improve the surface quality, refine grain size, and reduce segregation [1]. The flow and heat transfer in the continuous casting process are considerably complex so that it is impossible to study these issues by field tests because of a lack of the effective detecting methods. Moreover, experimental researches are expensive, time-consuming, and difficult to simulate the solidification process [2–4]. Numerical simulation was widely used to study and optimize the process [5–7]. Natarajan and El-Kaddah [8] researched the flow in rotary stirring of steel during casting with the finite element method. It was shown that the electromagnetic force (EMF) at the corners of the billet drove the molten steel to rotate. Two approaches to obtain the EMF were compared by Javurek et al. [9]: One was the semi-empirical method, and the other was calculation with the MHD module built into FLUENT. The results demonstrated that the semi-empirical method was suspectable, while FLUENT MHD module produced an overprediction of the EMF. Rywotycki et al. [10] analyzed the heat transfer of the billet in the mold and the secondary cooling zone, and the finite element method was employed to solve the equations. Song et al. [11, 12] took the joule heat produced by the M-EMS into account, and the results indicated that the Joule heat had little effect on the heat transfer. Geng et al. [13] considered that equiaxial crystal ratio was more impressionable to current intensity than to current frequency, namely, compared with improving current frequency, it is more effective to promote the equiaxial crystal ratio by improving current intensity.

The works published previously have laid a strong foundation of the researches on the M-EMS; however, quite few mathematical models took the solidification

✉ An-yuan Deng
dengay@epm.neu.edu.cn

[1] Key Laboratory of Electromagnetic Processing of Materials (Ministry of Education), Northeastern University, Shenyang 110004, Liaoning, China

[2] School of Metallurgy, Northeastern University, Shenyang 110004, Liaoning, China

process into account. In previous studies [14–17], most of the analysis has been performed on the driven flow; nevertheless, the solidification of the molten steel has huge influence on the flow. In addition, the emphasis was always put on the rotational flow of the molten steel on the horizontal cross section [18, 19]. In fact, the recirculation zone called secondary flow caused by the stirring is essential, and this phenomenon should be explored in detail to address its metallurgical effects. Moreover, in order to save the simulation time, the computational domain was usually restricted in the mold, whereas the fact that M-EMS has a strong effect on the whole billet was proved [20].

In this paper, based on the commercial software of ANSYS APDL and CFX, the user-defined procedures were developed for the solidification process so that a mathematical model containing magnetic field, heat transfer, flow, and solidification simultaneously was established to gain a deep insight into the flow and solidification of the billet with the M-EMS. Moreover, the emphases of present work were posed on the relationships of the stirring current to the rotational velocity, flow pattern in vertical direction, and mush zone of the billet. Besides, a comparison of the flow pattern with M-EMS between the models considering solidification and without considering solidification was conducted to show how solidification deeply influences the flow of molten steel. In addition, the modeling domain consisted of a billet up to 9.3 m from the meniscus, which exposed the effect of stirring current on the surface temperature of billet, the length of liquid core, and the thickness of solidified shell.

2 Mathematical model

2.1 Model assumptions

The following assumptions are made to simplify the numerical model:

1. The displacement current is neglected.
2. The flow and solidified shell of the steel have little effect on the magnetic field.
3. The meniscus is assumed flat, adiabatic, and the slag layer is not modeled.
4. The density, viscosity, specific heat, and thermal conductivity of steel are constant with temperature.
5. The influence of the mold oscillation on the billet is not considered.
6. The solidification shrinkage is irrespective.

2.2 Electromagnetic model

The magnetic field is analyzed by solving the Maxwell's equations with known boundary conditions. Maxwell's equations state that:

$$\nabla \cdot \boldsymbol{E} = \rho_{\mathrm{m}} \tag{1}$$

$$\nabla \cdot \boldsymbol{B} = 0 \tag{2}$$

$$\nabla \times \boldsymbol{E} = -\frac{\partial \boldsymbol{B}}{\partial t} \tag{3}$$

$$\nabla \times \boldsymbol{B} = \mu\left(\boldsymbol{J} + \frac{\partial \boldsymbol{E}}{\partial t}\right), \tag{4}$$

where $\boldsymbol{E}$ is the electric field strength; $\boldsymbol{B}$ is the magnetic flux density; $\boldsymbol{J}$ is the current density; μ is the magnetic permeability; ρ_{m} is the charge density; and t is the time.

In addition, another two equations can be written as:

$$\nabla \cdot \boldsymbol{J} = -\frac{\partial \rho_{\mathrm{e}}}{\partial t} \tag{5}$$

$$\boldsymbol{F} = q(\boldsymbol{E} + \boldsymbol{u} \times \boldsymbol{B}), \tag{6}$$

where $\boldsymbol{F}$ is the time-average Lorentz force acting on the molten steel; $\boldsymbol{u}$ is the velocity of molten steel; ρ_{e} is the total charge density; and q is the charge carried by every infinitesimal element.

For a continuous casting system, according to the MHD researches [21, 22], ρ_{m} plays no significant part, and the electric force, $q\boldsymbol{E}$, is negligible, compared with the Lorentz force. Besides, the influence of flow velocity on the magnetic field can be ignored. Thus, the Maxwell's equations can be simplified as:

$$\nabla \times \boldsymbol{H} = \boldsymbol{J} \tag{7}$$

$$\nabla \cdot \boldsymbol{J} = 0, \tag{8}$$

where $\boldsymbol{H}$ is the magnetic field intensity.

The constitutive equations are as follows:

$$\boldsymbol{B} = \mu \boldsymbol{H} \tag{9}$$

$$\boldsymbol{J} = \sigma \boldsymbol{E}, \tag{10}$$

where σ is the electric conductivity.

The time-average Lorentz force acting on the molten steel per unit volume $\boldsymbol{F}_{\mathrm{mag}}$ is expressed as follows:

$$\boldsymbol{F}_{\mathrm{mag}} = \frac{1}{2}\mathrm{Re}(\boldsymbol{J} \times \boldsymbol{B}), \tag{11}$$

where Re represents the real part.

2.3 Flow and solidification model

The process of the flow and solidification is simulated by solving continuity equation, Navier–Stokes equation, energy equation, and other supplementary equations. In

addition to the transport equations, the turbulent characteristic of the flow is defined by the k–ω model, which is more suitable in low Reynolds number flow than k–ε model [23, 24], where k is the turbulent kinetic energy; ω is the specific dissipation rate; and ε is the turbulent dissipation rate. The equations are expressed as follows:

$$\nabla \cdot \boldsymbol{u} = 0 \tag{12}$$

$$\nabla \cdot (\rho \boldsymbol{u}\boldsymbol{u}) = -\nabla P + (\mu_\mathrm{l} + \mu_\mathrm{t})\nabla^2 \boldsymbol{u} + \boldsymbol{F}_\mathrm{mag} + S_\mathrm{m} \tag{13}$$

$$\nabla \cdot (\rho \boldsymbol{u} k) = \nabla \cdot \left[\left(\mu_\mathrm{l} + \mu_\mathrm{t} + \frac{\mu_\mathrm{t}}{\sigma_k}\right)\nabla k\right] + G_k + S_k \tag{14}$$

$$\nabla \cdot (\rho \boldsymbol{u} \omega) = \nabla \cdot \left[\left(\mu_\mathrm{l} + \mu_\mathrm{t} + \frac{\mu_\mathrm{t}}{\sigma_\omega}\right)\nabla \omega\right] + G_\omega + S_\omega, \tag{15}$$

where P is pressure; ρ is the density of molten steel; μ_l and μ_t are molecular viscosity and turbulent viscosity, respectively; G_k and G_ω represent the generation of turbulence kinetic energy and specific dissipation rate, respectively; σ_k and σ_ω are the Prandtl numbers corresponding to the turbulent kinetic energy and the turbulent energy dissipation rate, respectively; and S_m, S_k, S_ω are source items.

In the model, the mush zone in the billet is regarded as porous media, in which the turbulence flow is damped. As a result, it must be taken into account by adding source terms S_m and S_ϕ ($\phi = k$, ω) into the Navier–Stokes equation and the governing equations of turbulence model. According to the Darcy's law, it can be expressed as [25–27]:

$$S_\mathrm{m} = -\mu_\mathrm{l}\frac{(1-f_\mathrm{l})^2}{(f_\mathrm{l}^3 + \xi)}\frac{180}{\lambda_2^2}(\boldsymbol{u} - \boldsymbol{u}_\mathrm{c}) \tag{16}$$

$$S_\phi = -\mu_\mathrm{l}\frac{(1-f_\mathrm{l})^2}{(f_\mathrm{l}^3 + \xi)}\frac{180}{\lambda_2^2}\phi, \tag{17}$$

where ξ is a constant less than 0.0001; λ_2 is the secondary dendrite arm spacing; $\boldsymbol{u}_\mathrm{c}$ is the casting velocity; and f_l is the liquid fraction defined as:

$$f_\mathrm{l} = \begin{cases} 0 & T \le T_\mathrm{s} \\ 1 & T \ge T_\mathrm{l} \\ \dfrac{T - T_\mathrm{s}}{T_\mathrm{l} - T_\mathrm{s}} & T_\mathrm{s} < T < T_\mathrm{l} \end{cases}, \tag{18}$$

where T is the temperature of molten steel; T_s is the solidus temperature; and T_l is the liquidus temperature.

The energy equation is written as:

$$\nabla \cdot (\rho \boldsymbol{u} H) = \nabla \cdot (\lambda_\mathrm{eff}\nabla H) + \nabla \cdot [\lambda_\mathrm{eff}\nabla(h_\mathrm{s} - H)] - \nabla \cdot [\rho(\boldsymbol{u} - \boldsymbol{u}_\mathrm{c})(h_\mathrm{l} - H)], \tag{19}$$

where H is the total enthalpy; h_s is the enthalpy of solid phase; h_l is the enthalpy of liquid phase; and λ_eff is the effective thermal conductivity.

The constitutive equations are as follows:

$$H = h_\mathrm{ref} + \int_{T_\mathrm{ref}}^{T_\mathrm{tim}} c_p \,\mathrm{d}T + f_\mathrm{l} L \tag{20}$$

$$\lambda_\mathrm{eff} = \frac{\mu_\mathrm{l}}{Pr} + \frac{\mu_\mathrm{t}}{Pr_\mathrm{t}}, \tag{21}$$

where Pr and Pr_t are the Prandtl number and turbulent Prandtl number, respectively; h_ref is the reference enthalpy; T_ref is reference temperature; T_tim is the timely temperature of the molten steel; c_p is the specific heat of molten steel; and L is latent heat.

2.4 Boundary conditions

Uniform velocity determined by mass conservation is applied at the nozzle inlet, and the turbulence parameters are estimated by Eqs. (22) and (23):

$$k_\mathrm{in} = 0.01 v_\mathrm{in}^2 \tag{22}$$

$$\varepsilon_\mathrm{in} = \frac{2k_\mathrm{in}^{1.5}}{d_0}, \tag{23}$$

where v_in is the velocity of molten steel at inlet; d_0 is the diameter of inlet; and subscript in indicates the nozzle inlet.

The normal gradients of all variables are set equal to zero at the meniscus and outlet. Moreover, the velocity perpendicular to meniscus is also equal to zero. The wall of the billet is treated as moving wall, whose velocity is specified as casting velocity.

The heat transfer between external environment and liquid steel in the mold is complex. Therefore, the heat transfer boundary condition applied in mold is simplified as mean heat flux, and it is expressed as follows:

$$q_\mathrm{m} = \left(268 - \beta\sqrt{\frac{l}{u_\mathrm{c}}}\right) \times 10^4 \tag{24}$$

$$\beta = \frac{1.5 \times (2{,}680{,}000 - \overline{q})}{\sqrt{L_\mathrm{m}/u_\mathrm{c}}} \tag{25}$$

$$\overline{q} = \frac{\rho_\mathrm{w} C_\mathrm{w} W_\mathrm{L} \Delta T}{S_\mathrm{c}}, \tag{26}$$

where q_m is the heat flux of the mold; l is the distance of molten steel from meniscus; β is an empirical coefficient; L_m is the effective length of the mold; $\bar{q}$ is the mean heat flux of the mold; ρ_w is the density of cooling water; C_w is the specific heat of cooling water; W_L is the flow rate of cooling water located in mold; ΔT is the temperature difference of cooling water between inlet and outlet of the

mold cooling system; and S_c is the effective contact surface between mold wall and molten steel.

The convection boundary and radiation boundary conditions are applied at secondary cooling zone and air cooling zone, respectively, and it can be calculated by Eqs. (27) and (28):

$$q_S = \frac{1.57W_2^{0.57}(1 - 0.0075t_w)}{\alpha}(T_{sur} - T_w) \quad (27)$$

$$q_a = \varepsilon_r \sigma_B \left(T_{sur}^4 - T_w^4\right), \quad (28)$$

where q_S is the heat flux of secondary cooling zone; W_2 is the spray water flux; t_w is the temperature of cooling water; α is a coefficient related to guide roller; T_{sur} and T_w are the surface temperature of billet and environment temperature, respectively; q_a is the heat flux of air cooling zone; ε_r is the radiation heat transfer coefficient; and σ_B is the Boltzmann constant.

2.5 Numerical methods and geometric model

Based on the commercial software CFX and the Fortran program compiled in advance, the finite volume method was used to solve the governing equations of flow and heat transfer. The high-resolution interpolation method was used as the advection scheme. The convergence was considered satisfactory when the average residual target of 1×10^{-4} was obtained and the sum of mass residual in all nodes was less than 0.01% of the initial total mass. All calculation was done in steady state to save computation time. The geometric model of the billet and M-EMS is represented in Fig. 1. The main material properties and operating parameters are listed in Table 1.

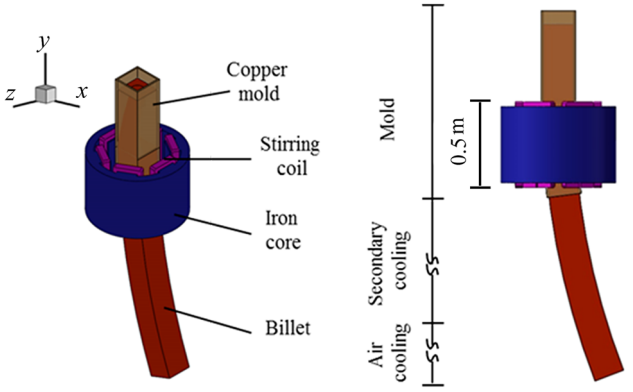

Fig. 1 Diagram of billet and M-EMS

Table 1 Properties of molten steel and process parameters used in calculation

Parameter	Value
Conductivity/(S m^{-1})	7.14×10^5
Relative permeability	1
Density/(kg m^{-3})	7100
Viscosity/(Pa s)	6.7×10^{-3}
Specific heat/(J kg^{-1} K^{-1})	643.8
Thermal conductivity/(W m^{-1} K^{-1})	30
Latent heat/(J kg^{-1})	2.556×10^5
Solidus temperature/K	1751.15
Liquidus temperature/K	1663.15
Casting temperature/K	1767.15
Ambient temperature/K	300
Casting velocity/(m min^{-1})	1.75
Cross-sectional dimensions/(m × m)	0.16 × 0.16
Radius of caster/m	10
Length of mold/m	1
Length of billet/m	9.3

3 Results and discussion

3.1 Model validation

Reliability verification is essential for the mathematical simulation. Although the characteristics of electromagnetic field are not discussed in this paper, it is the basis of present work and the accuracy of electromagnetic model should be proved definitely. In order to validate it, a comparison of the calculated and measured magnetic flux densities along the central axis of the stirrer, which is obtained by a CT-3 Tesla-meter in the mold without charge, is conducted. It is obvious that the calculated data agree well with the measured ones as shown in Fig. 2, and the former is a little

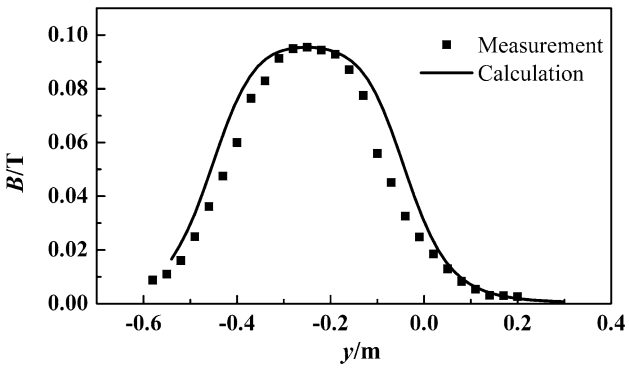

Fig. 2 Comparison of measured and calculated magnetic induction densities along central axis of stirrer

larger than the latter, which is due to the overlook of magnetic loss.

The solidification process, such as the length of liquid core and the thickness of solidified shell, attracts attention of most metallurgical engineers. Therefore, one of the approaches for validating the solidification model is to compare the calculated and measured solidified shell thickness. In the current work, the nail experiments have been conducted under different conditions to assess the thickness of the solidified shell. Figure 3 shows the sulfur print results of the nail experiments for the cases of casting speed about 1.75 m/min and 1.90 m/min. The measured thickness of solidified shell l_1 and l_2 is 69.76 mm and 63.30 mm, respectively. The comparison of the calculated and measured solidified shell thickness is shown in Fig. 4. It can be seen that the calculated and measured values are in good agreement. Besides, this model is also validated by comparing with the experiments conducted by Deng and He [28].

3.2 Distribution of Lorentz force

The flow and solidification of molten steel are definitely affected by the distribution of the Lorentz force; hence, the discussion about the Lorentz force is essential. Figure 5 shows the distribution of the Lorentz force on the transverse and longitudinal cross section of the billet. It can be seen that the Lorentz force rotates on the transverse cross section, and it gradually increases from the center to the surface of the billet, which may force the molten steel to rotate on the transverse cross section. The distribution that Lorentz force increases first and then decreases along the longitudinal direction will cause secondary flow undoubtedly. The simulation about the flow of molten steel without considering solidification process has been reported in many researches; even so, it is crucial to take the solidification into account, because the solidification can easily affect the flow of molten steel, especially in the zone near the solidification front.

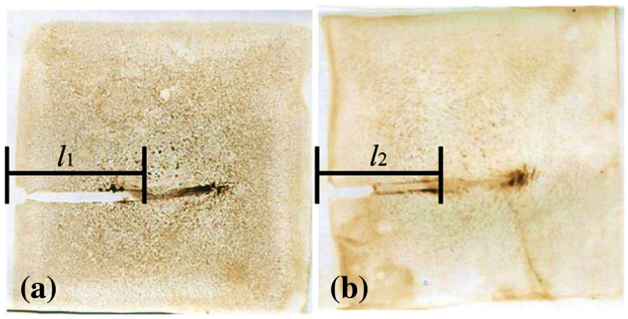

Fig. 3 Sulfur print of nail experiments

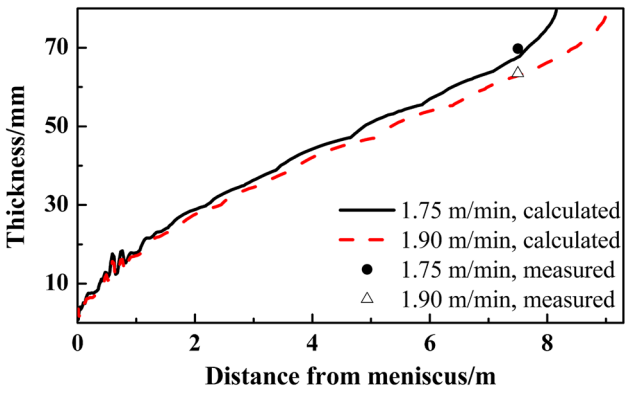

Fig. 4 Comparison of calculated and measured solidified shell thickness

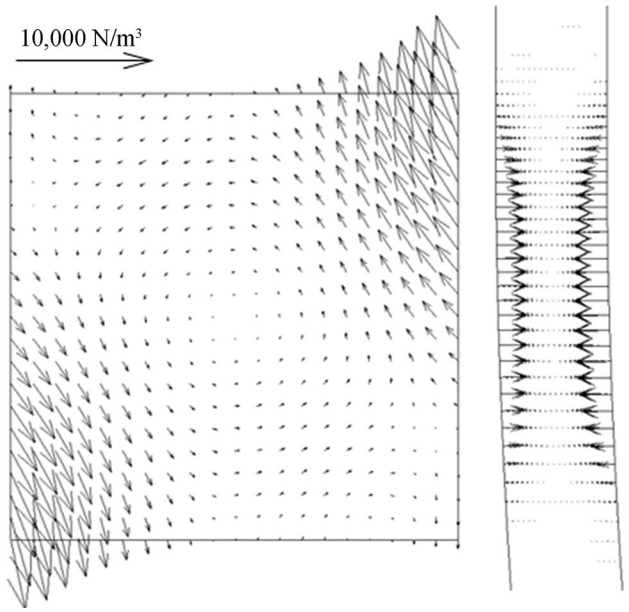

Fig. 5 Distribution of Lorentz force on transverse and longitudinal cross section

3.3 Flow and solidification around the stirrer

The M-EMS affects the flow of molten steel first and then indirectly influences the heat transfer and solidification. Figure 6 reveals the change of the flow on the transverse cross section. It can be observed that the velocity of molten steel is the same as the casting velocity without the M-EMS, and there is no tangential velocity. However, when the electromagnetic stirring is applied, the molten steel is affected by the rotating electromagnetic force, resulting in a strong rotation, and its rotational velocity increases with the increase in current intensity. Figure 7 shows the variation of the velocity with different current intensities at 4 Hz over the width of the billet on the central cross section of the stirrer. It is obvious that the velocity of molten steel increases with increasing current intensity.

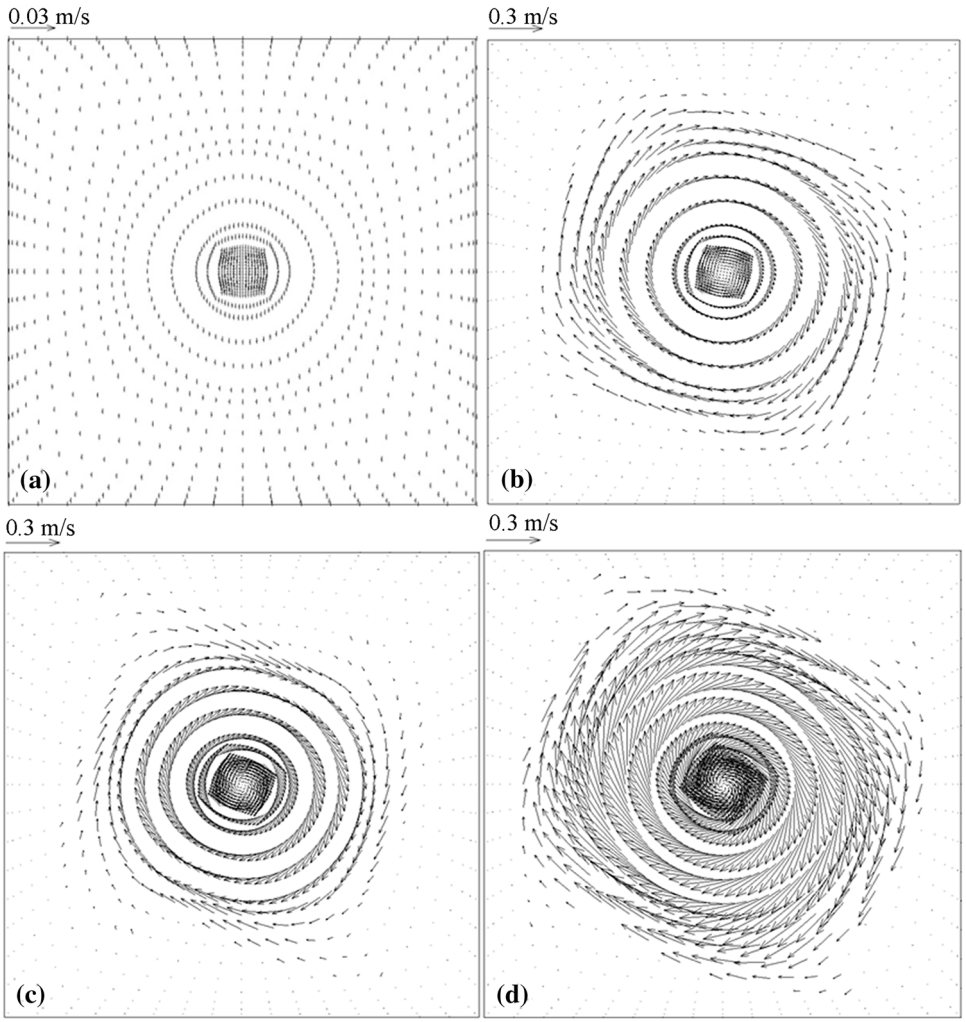

Fig. 6 Velocity distribution on central cross section of stirrer with different current intensities. **a** 0 A; **b** 320 A; **c** 452 A; **d** 640 A

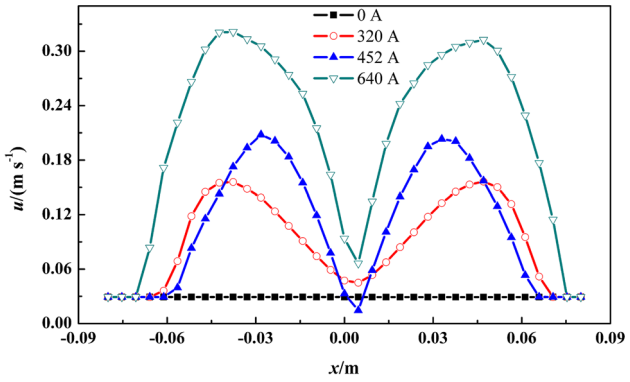

Fig. 7 Variation of velocity with different current intensities

The maximum velocity is proportional to the current intensity, and the maximum velocity reaches 0.32 m/s when the current intensity reaches 640 A. Moreover, the velocity increases firstly and then decreases from the center to the surface of the billet. There are two factors contributing to this situation. One of them is that the electromagnetic force increases gradually from the center to the surface of the billet, and the other is that the velocity is damped due to the solidification.

Some researchers [21, 29, 30] pointed out that compared with conventional continuous casting process, two vortexes called secondary flow phenomenon affected by the axial gradient of electromagnetic force appeared in the lower area of the mold except for the other two near the submerged entry nozzle (SEN). The velocity vector of the billet on the central longitudinal section is shown in Fig. 8. In the absence of the M-EMS, the molten steel flows into the liquid pool from the SEN with high speed and forms two symmetrical vortexes on both sides of the mainstream. When the stream of molten steel reaches the center or lower section of the mold, the flow tends to be stable, and the velocity is the same as the casting velocity. After the M-EMS being adopted, the penetration depth of the molten steel stream, to some extent, is reduced and gradually

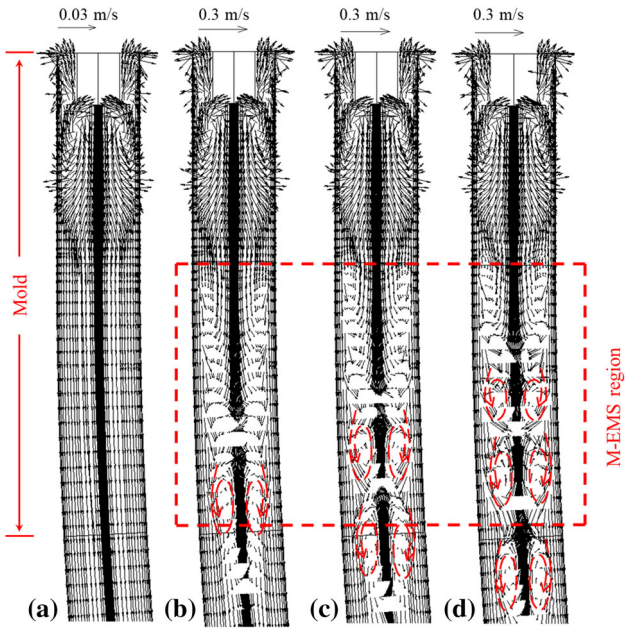

Fig. 8 Velocity distribution of molten steel on central vertical section with different current intensities. **a** 0 A; **b** 320 A; **c** 452 A; **d** 640 A

descends with the increase in the current intensity. In addition, owing to the gradient of the axial electromagnetic force, the secondary flow phenomenon comes into being. However, compared with previous researches [21, 29, 30] which show that only a pair of vortexes is generated, more than two vortexes appear within the lower half region of the stirrer. It can be clearly seen that only a pair of vortexes is generated with current intensity of 320 A, while the number of vortexes rises to 4 and 6 when the current intensity reaches 452 A and 640 A, respectively. In the preceding studies [21, 29, 30], the agitation strength may not be strong enough to cause two or more pairs of whirlpools. A comparison of maximum rotational velocity caused by the M-EMS between this study and the others [21, 29, 30] negates this conjecture, because there is still only a pair of vortexes when the maximum rotational velocity reaches 0.3 m/s [31]. This finding suggests that the number of vortexes is affected by the stirring parameters, that is, it is not limited to two, and it may change the solidification process.

The actuating range of the M-EMS is not usually confined to the area encompassed by the stirrer, and it depends on the current to a large extent. Thus, it is crucial to determine the effective area of the M-EMS. Figure 9 shows the variation of the maximum tangential velocity without and with M-EMS, with current of 320 A and frequency of 4 Hz. It can be seen that the stirring has little influence on the tangential motion of the molten steel within the vertical range of 0.32 m from the meniscus, and the tangential velocity is mainly caused by the free jet. Tangential

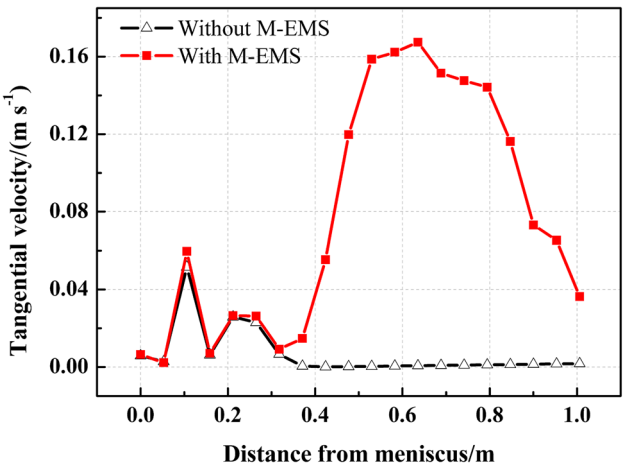

Fig. 9 Maximum tangential velocity distribution of molten steel along axis of casting

velocity is almost zero without M-EMS when beyond that range. However, when M-EMS is applied, affected by the electromagnetic stirring, the tangential velocity of the molten steel goes up with the increase in the distance from the meniscus and peaks appear at 0.17 m/s near the central cross section of the stirrer. Then, the tangential velocity drops off, and it is still 0.07 m/s at the outlet of the mold. In this way, the effective area of the M-EMS can be obtained.

The solidification of billet can be changed dramatically by the M-EMS. Figure 10 shows that the thickness of solidified shell fluctuates within the effective area of the stirrer. The underlying cause for this phenomenon is the unsteady erosion to the solidification front caused by the

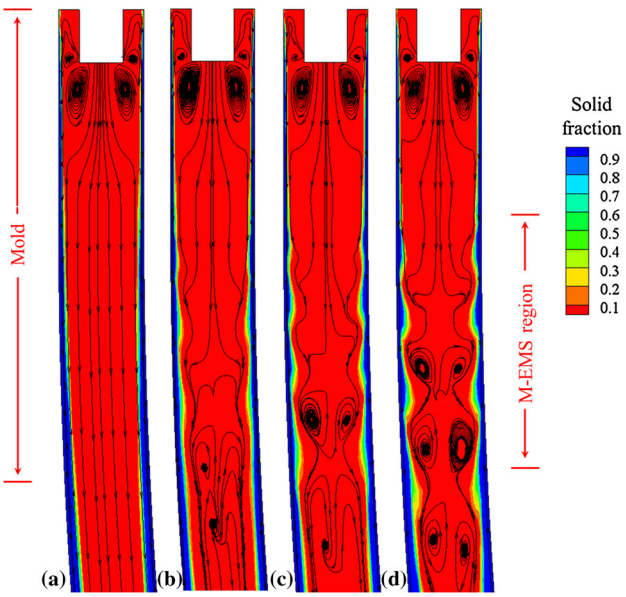

Fig. 10 Streamlines and contour of solidification on central vertical section with different current intensities. **a** 0 A; **b** 320 A; **c** 452 A; **d** 640 A

unsteady flow of the molten steel. It can be observed in Fig. 10 that the vortexes caused by stirring are located in the weak areas of the solidified shell. Moreover, the immediate cause is that the M-EMS improves the heat transfer conditions in the liquid pool. As shown in Fig. 11, on one hand, the forced convection of the molten steel promotes the scour to the solidification front, which reduces the thickness of the solidified shell; on the other hand, the forced convection also weakens the temperature gradient near the solidifying front, which accelerates the solidification. Above all, the fluctuation of the solidified shell thickness occurred.

As mentioned above, the unsteady erosion to the solidification front caused by the unsteady flow of the molten steel, such as the vortexes located in the lower half of the stirrer, leads to the fluctuation of the solidified shell thickness within the effective stirring area. In fact, not only the stirrer produces the vortexes, but also the solidification has a great influence on the flow pattern of the molten steel. Nevertheless, the effect of the solidification on the flow pattern was not considered in most previous numerical simulation researches. The difference of flow pattern with and without considering the solidification is shown in Fig. 12. It can be observed that the penetration depth and the upper swirl zone on both sides of the mainstream become smaller obviously. Besides, three pairs of vortexes are generated in the lower half area of the stirrer, when the solidification is considered in the mathematical model. In contrast, the flow pattern of the molten steel varies significantly when the solidification is neglected. One of the changes is that the upper swirl zone gets larger and the

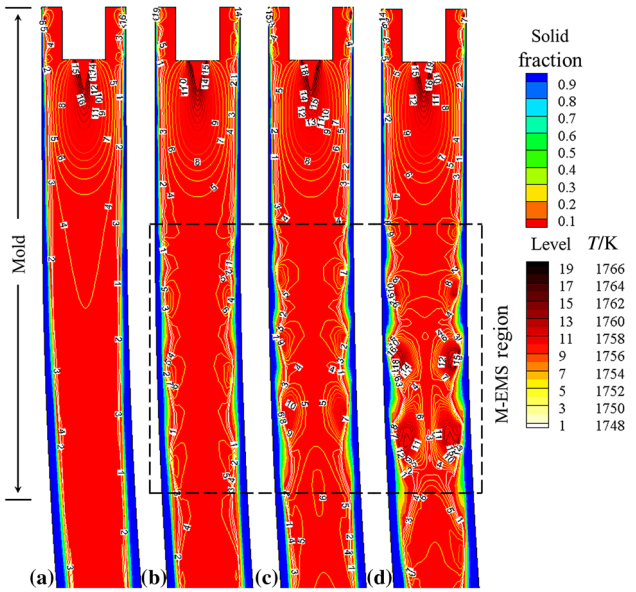

Fig. 11 Isotherm and contour of solidification on central vertical section with different current intensities. **a** 0 A; **b** 320 A; **c** 452 A; **d** 640 A

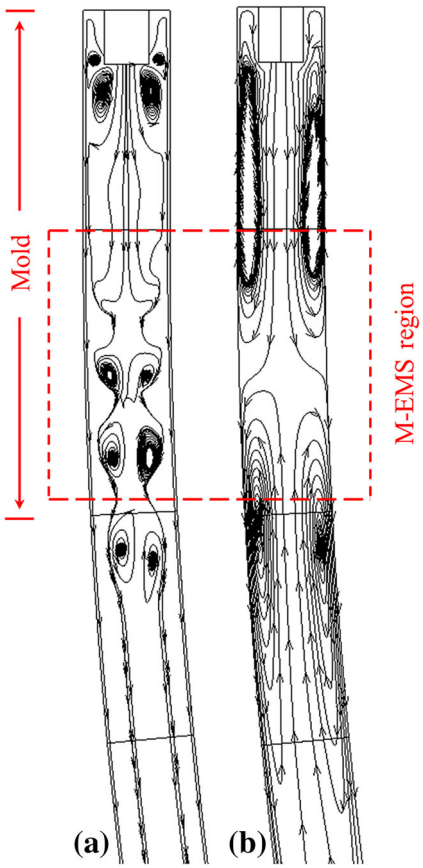

Fig. 12 Streamlines on central vertical section with (**a**) and without (**b**) solidification

penetration depth reduces; the other one is that only a pair of huge vortexes appears near the outlet of the mold. This result indicates that the flow pattern, temperature distribution, and solidification affect each other and are inseparable; therefore, the solidification must be considered when the numerical simulation of the continuous cast is conducted.

The solidification status of billet at the outlet of the mold is greatly concerned by researchers. Figure 13 shows the distribution of the solidification fraction. It can be seen that the molten steel in the mold can solidify uniformly, and the solidified shell is regular when the M-EMS is not applied. If the M-EMS is applied, the location of the solidification front will change a lot because of the rotation of the molten steel, and the perturbation of the molten steel to the shell goes up with the increase in the current intensity. When the current intensity increases from 320 to 452 A, the shape of the solidified shell does not change clearly. When the current intensity reaches 640 A, the area of liquid phase gets clearly more narrow and tends to be round; besides, the mush zone expands, which will promote the growth of the equiaxed grains [32]. It can be concluded that only when the rotational velocity of the molten steel is increased

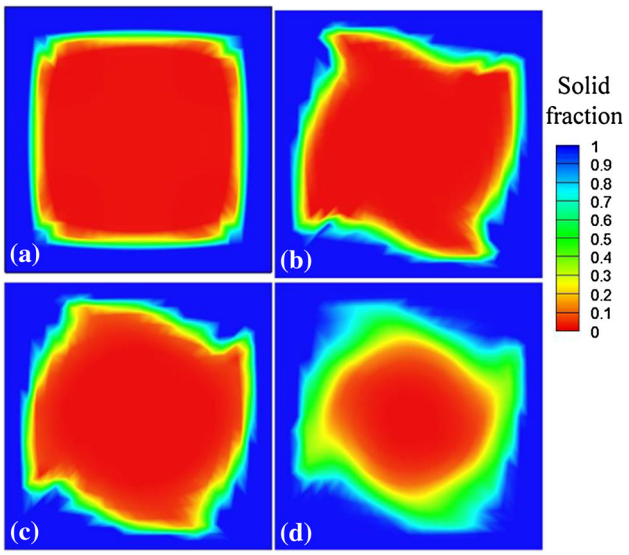

Fig. 13 Solid fraction at exit of mold with different current intensities. **a** 0 A; **b** 320 A; **c** 452 A; **d** 640 A

to 0.3 m/s or more, could the M-EMS promote the convective heat transfer of molten steel and the development of equiaxed crystal at the same time.

As stated above, the solidified shell changes a lot within the effective area of the stirrer, and it gets irregular, whereas the transformation is eliminated gradually by the process of solidification. Figure 14 shows the phase distribution on different cross sections with different current intensities. It can be observed that although the shell within the effective area of the stirrer is distorted, it becomes regular and symmetrical again; when the billet leaves the foot rollers, especially for the billet stirring current of 640 A, this phenomenon gets more apparent. In addition, the mush zone expands obviously with the M-EMS, and it ascends with the increase in current intensity. It is easy to come up with a conclusion that when the current intensity reaches 640 A, that is, when the rotational velocity of the molten steel gets to 0.3 m/s or more, the effect of the M-EMS on the expansion of the mush zone will be very significant. In fact, some studies have shown that the maximum diameter of the clusters remaining in the billet is corresponding to the rotational velocity, and the inclusions with a size of 100 μm can be prevented from embedding into the solidified shell by increasing the flow velocity of molten steel to 0.3 m/s [33, 34].

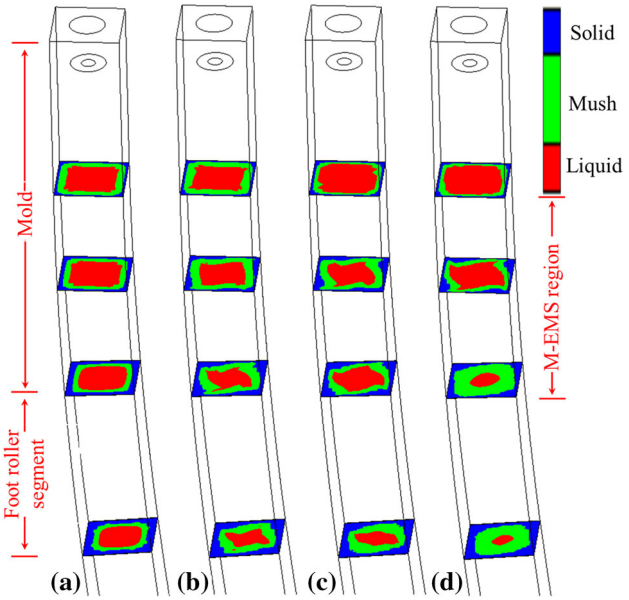

Fig. 14 Phase distribution on different cross sections with different current intensities. **a** 0 A; **b** 320 A; **c** 452 A; **d** 640 A

3.4 Solidification of whole billet

Although the M-EMS changes the flow of the molten steel only within the effective region, it has an effect on the solidification behavior in the whole billet. Figures 15 and 16 show the variation of the thickness of the solidified shell and the surface temperature along the billet, respectively. It can be found that both of them fluctuate within the mold section and the foot roller section with the M-EMS, and the surface temperature in these areas increases significantly (it rises about 100–150 K), which indicates that the M-EMS does improve the heat transfer condition of the billet, therefore accelerating the solidification of the molten steel and shortening the length of liquid core. The M-EMS changes the solidification process of the billet; moreover, the situation also varies with the stirring current. Compared with the casting process without the M-EMS, the surface temperature within the mold section and the foot roller section rises about 100 K, and the average increase in the thickness of the solidified shell is about 1 mm for the two processes with the stirring current of 320 A and 452 A. This situation changes when the current intensity reaches 640 A. In this condition, the fluctuation of the surface temperature and the thickness of the solidified shell within the lower half of the mold intensify. Meanwhile, the

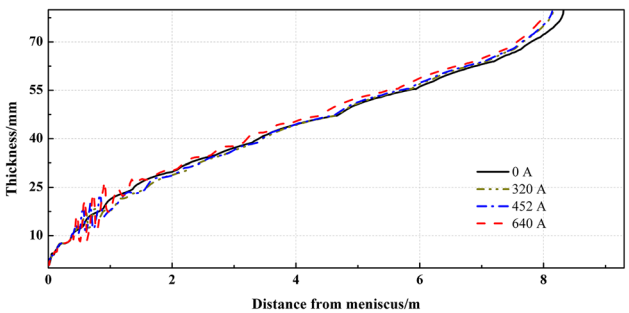

Fig. 15 Shell thickness distribution of billet with different current intensities

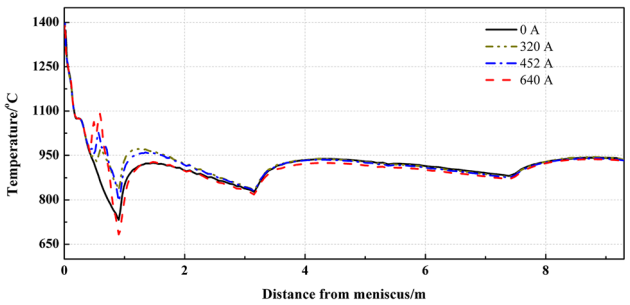

Fig. 16 Distribution of temperature on surface with different current intensities

surface temperature of the billet is further reduced; when the current intensity is 320, 452, and 640 A, the surface temperature drop is about 3, 5, and 12 K, respectively. Correspondingly, the thickness of the solidified shell at the same location increases and the length of liquid core gets shorter, which is about 8.32, 8.16, 8.13, and 8.02 m for the stirring current of 0, 320, 452, and 640 A, respectively. This phenomenon indicates that significant changes happened within the solidification process when the current intensity reaches 640 A, and this current intensity can be a critical value for the casting process.

4 Conclusions

1. When the M-EMS is applied, the flow pattern of the molten steel on the cross section is rotary, and the velocity of the billet increases firstly and then decreases from the center to the surface. Moreover, the rotational velocity goes up with the increase in the current intensity, and the maximum velocity reaches 0.32 m/s when the current intensity reaches 640 A.
2. The flow pattern of the molten steel on the transverse and longitudinal cross sections is changed by the M-EMS. The number of the vortexes within the lower swirl zone is related to the current intensity. The service area of the stirrer can be obtained accurately by investigating the maximum tangential speed of the molten steel along the casting direction of the billet.
3. The thickness and the shape of the solidified shell fluctuate within the effective area of the stirrer with the M-EMS, and the fluctuation is restricted to the lower half of the mold and the foot roller section. Moreover, because of the improvement in the heat transfer condition, the mush zone expands, which will promote the increase in the equiaxed crystal ratio, accelerate the solidification process, and shorten the length of liquid core. Compared with the stirring current intensity of 320 A and 452 A, when the current intensity reaches 640 A, namely, when the maximum rotational velocity reaches 0.32 m/s, the liquid region shrinks, the mush zone enlarges, and the solidification process is obviously different from the others. It is essential to obtain an appropriate current intensity to improve the quality of the billet by using the M-EMS.
4. The flow, heat transfer, and solidification of the molten steel are closely correlated; therefore, the solidification must be considered when the numerical simulation about the continuous casting process is conducted.

Acknowledgements This work was supported by National Natural Science Foundation of China (51474065, 51574083), the Doctoral Scientific Research Foundation of Liaoning Province of China (20141008), and the Program of Introducing Talents of Discipline to Universities of China (B07015).

References

[1] K. Fujisaki, T. Ueyama, T. Toh, M. Uehara, S. Kobayashi, IEEE Trans. Magn. 34 (1998) 2120–2122.
[2] J. Partinen, N. Saluja, J. Szekely, J. Kirtley Jr., ISIJ Int. 34 (1994) 707–714.
[3] J. Partinen, J. Szekely, C. Vives, L. Holappa, ISIJ Int. 35 (1995) 292–301.
[4] B. Willers, M. Barna, J. Reiter, S. Eckert, ISIJ Int. 57 (2017) 468–477.
[5] K.C. Mills, P. Ramirez-Lopez, P.D. Lee, B. Santillana, B.G. Thomas, R. Morales, Ironmak. Steelmak. 41 (2014) 242–249.
[6] B. Wang, Z.G. Yang, X.F. Zhang, Y.T. Wang, C.P. Nie, Q. Liu, H.B. Dong, Metalurgija 54 (2015) 327–330.
[7] M. Barna, M. Javurek, J. Reiter, M. Lechner, BHM Berg-und Hüttenmännische Monatshefte 154 (2009) 518–522.
[8] T.T. Natarajan, N. El-Kaddah, Appl. Math. Model. 28 (2004) 47–61.
[9] M. Javurek, M. Barna, P. Gittler, K. Rockenschaub, M. Lechner, Steel Res. Int. 79 (2008) 617–626.
[10] M. Rywotycki, Z. Malinowski, J. Giełżecki, A. Gołdasz, Arch. Metall. Mater. 59 (2014) 487–492.
[11] X.P. Song, S.S. Cheng, Z.J. Cheng, J. Iron Steel Res. Int. 19 (2012) No. S2, 983–986.
[12] X.P. Song, S.S. Cheng, Z.J. Cheng, Ironmak. Steelmak. 40 (2013) 189–198.
[13] X. Geng, X. Li, F.B. Liu, H.B. Li, Z.H. Jiang, Ironmak. Steelmak. 42 (2015) 675–682.
[14] B.A. Sivak, V.G. Grachev, V.M. Parshin, A.D. Chertov, S.V. Zarubin, V.G. Fisenko, A.A. Solov'ev, Metallurgist 53 (2009) 469–481.
[15] H.Q. Yu, M.Y. Zhu, IEEE Trans. Magn. 46 (2010) 82–86.
[16] H.P. Liu, M.G. Xu, S.T. Qiu, H. Zhang, Metall. Mater. Trans. B 43 (2012) 1657–1675.
[17] J. Gong, H.P. Liu, X.H. Wang, Y.P. Bao, J. Iron Steel Res. Int. 22 (2015) 414–422.

[18] B.Z. Ren, D.F. Chen, H.D. Wang, M.J. Long, Z.W. Han, Ironmak. Steelmak. 42 (2015) 401–408.
[19] B.Z. Ren, D.F. Chen, H.D. Wang, M.J. Long, Steel Res. Int. 86 (2015) 1104–1115.
[20] D.B. Jiang, M.Y. Zhu, Steel Res. Int. 86 (2015) 993–1003.
[21] P.A. Davidson, F. Boysan, Appl. Sci. Res. 44 (1987) 241–259.
[22] T. Robinson, K. Larsson, J. Fluid Mech. 60 (1973) 641–664.
[23] A.Y. Deng, J.C. He, Acta Metall. Sin. (Engl. Lett.) 15 (2002) 471–478.
[24] P.T. Hietanen, S. Louhenkilpi, S. Yu, Steel Res. Int. 88 (2017) 1600355.
[25] V.R. Voller, J. Cryst. Growth 197 (1999) 325–332.
[26] I. Farup, A. Mo, Metall. Mater. Trans. A 31 (2000) 1461–1472.
[27] S. Luo, F.Y. Piao, D.B. Jiang, W.L. Wang, M.Y. Zhu, J. Iron Steel Res. Int. 21 (2014) No. S1, 51–55.
[28] A.Y. Deng, J.C. He, Research on Iron and Steel (2000) No. 1, 15–18.
[29] D.J. Im, J.S. Hong, I.S. Kang, Comput. Fluids 70 (2012) 13–20.
[30] A. Maurya, P.K. Jha, Appl. Math. Model. 48 (2017) 736–748.
[31] Z.G. Yang, B. Wang, X.F. Zhang, Y.T. Wang, H.B. Dong, Q. Liu, J. Iron Steel Res. Int. 21 (2014) 1095–1103.
[32] B. Mao, G.F. Zhang, A.W. Li, Theory and technology of electromagnetic stirring for continuous casting, Metallurgical Industry Press, Beijing, 2012.
[33] T. Matsumiya, ISIJ Int. 46 (2006) 1800–1804.
[34] W. Yamada, CAMP-ISIJ 12 (1999) 682–684.